Hemp hurd torrefaction as an effective strategy to enhance PLA-based composite mechanical and tribological properties

scientific reports

Check for updates

OPEN

Hemp hurd torrefaction as an effective strategy to enhance PLA-based composite mechanical and tribological properties

Paola Brachi[1], Giovanna Ruoppolo[1], Maria Giulia Faga[2], Mattia Di Maro[2]✉, Giulio Malucelli[3] & Donatella Duraccio[2]

Torrefied hemp hurd (HH) was investigated as a sustainable filler for poly (lactic acid) (PLA)-based composites. HH, a byproduct of the textile industry, underwent torrefaction at 220, 260, and 300 °C to enhance its compatibility with PLA. The resulting fillers (HH220, HH260, HH300) were characterized in terms of morphology, structure, and thermochemical properties. Composites incorporating 2.5 and 5 wt% of each torrefied filler were prepared via melt mixing and characterized for their structural, thermal, mechanical, and tribological behavior. SEM analysis revealed that higher torrefaction temperatures resulted in improved filler dispersion and adhesion to the PLA matrix. While all composites exhibited reduced ductility (i.e., elongation at break), those containing HH300 demonstrated the highest increases in Young's modulus, tensile strength, hardness, and wear resistance. Notably, the HH300 composite containing 5 wt% showed significant improvements over unfilled PLA, including increased stiffness (+12%) and toughness (+27%), as well as substantial reductions in coefficient of friction (– 83%), and wear rate, that is reduced by about three orders of magnitude. Finally, when compared to the composite containing untreated hemp hurd, stiffness increased by 24%, toughness by 78%, with wear rate still reduced by about three orders of magnitude and friction coefficient lowered by 80%. Torrefied hemp hurd, especially when treated at high temperatures, is thus a promising bio-based reinforcement that improves the performance of PLA composites in structural and tribological applications.

Keywords Polylactic acid, Hemp hurd, torrefaction, mechanical behavior, Tribological properties

Hemp is a highly adaptable crop with a long history of cultivation, valued not only for its industrial fiber applications-especially in textiles-but also for its agronomic benefits[1,2]. It grows quickly across a range of soil conditions and climates, typically maturing within 100 days and demanding relatively low inputs like water and fertilizers. For these reasons, it is a perfect candidate for sustainable farming practices. Hurd, the woody inner portion of the hemp stalk, is separated during the fiber production process and can be repurposed for a range of sustainable applications, including animal bedding, eco-friendly construction materials (i.e., hempcrete, biodegradable packaging, erosion control products, paper production), and even as a feedstock for bioenergy, bio-oil, or compost[3–5]. Nonetheless, a significant amount of hurd residues continues to be discarded in landfills, highlighting the need for innovative and sustainable uses of this underutilized resource[6]. Compared to synthetic or mineral-based fillers, hurd offers numerous benefits, including lower production costs and reduced material density. Moreover, it contributes to energy-efficient processing and poses fewer health concerns. Its inherent properties - such as renewability, biodegradability, and potential for recycling-further enhance its environmental appeal, while also helping to mitigate landfill accumulation[7–10]. The hydrophilic nature of hurd limits its compatibility with hydrophobic polymers, hindering its effectiveness as a filler in composites. Since strong filler-matrix adhesion is essential for stress transfer in composites[11], various methods have been explored, such as the enzymatic modification, the use of graft co-polymers, and of a coupling agent to improve the mechanical and thermal properties of the resulting composites[10,12,13]. However, these treatments can pose environmental

[1]Istituto di Scienze e Tecnologie per l'Energia e la Mobilità Sostenibili, Consiglio Nazionale delle Ricerche, P. le V. Tecchio, 80-80125 Naples, Italy. [2]Istituto di Scienze e Tecnologie per l'Energia e la Mobilità Sostenibili, Consiglio Nazionale delle Ricerche, Strada delle Cacce, 73-1035 Turin, Italy. [3]Dipartimento di Scienza Applicata e Tecnologia, Politecnico di Torino, Viale Teresa Michel 5, 15121 Alessandria, Italy. ✉email: mattia.dimaro@stems.cnr.it

concerns due to the use of solvents. Torrefaction is a well-known process involving the thermal treatment of biomass at temperatures between 200 and 300 °C in an oxygen-free environment[14]. The final material properties depend on the temperature, heating rate, and residence time[15]. Compared to pyrolysis, which produces syngas and bio-oil and necessitates complex gas management systems, torrefaction yields fewer volatile compounds and is operationally simpler. This process presents new opportunities for adding value to agricultural residues and enhancing the sustainability of supply chains. Torrefied biomass exhibits improved characteristics, including higher hydrophobicity, higher energy content, easier grindability, and lower moisture absorption - features that contribute to better storage stability and handling[16]. Enhanced hydrophobicity is particularly beneficial in polymer composite applications, as it improves interfacial adhesion between the filler and the matrix. Indeed, incorporating torrefied biomass into polymer composites not only adds value to waste materials and reduces the plastic content but also influences the mechanical and thermal performance of the resulting materials. In the literature, various biomasses and byproducts have been subjected to torrefaction for the purpose of enhancing their compatibility and performance in polymer composite systems. The resulting properties of such torrefied biomass-polymer composites - particularly their mechanical and thermal characteristics - have thoroughly been investigated[17–25].

For instance, Vold et al.[17] found that incorporating torrefied sunflower hulls and flax shives into polyamide gave rise to composites with tensile and flexural strengths that were 70% and 94% of the unfilled matrix, respectively. The composites also showed increased elastic and flexural modulus by about 150% and decreased moisture absorption by as much as 50%. McCaffrey et al.[19] showed that torrefied almond shell can be effectively incorporated into polypropylene-polyethylene (PP-PE) blends without the need for a compatibilizer. Their findings indicated that increasing the filler content enhanced the flexural and tensile moduli, while simultaneously reducing the material's strength, elongation at break, and toughness. Additionally, the maximum improvement in heat distortion temperature (HDT) was observed at a 30 wt% loading of small particles, showing an increase of 10 °C compared to the unfilled blend. Among the biodegradable polymers studied, poly(lactic acid) (PLA)[21,23] and polyhydroxybutyrate (PHB)[22] were reinforced using torrefied coffee husk, larch wood and rice husk, respectively. Specifically, injection-molded PLA composites containing 20 wt% torrefied coffee husk exhibited enhanced mechanical properties, as determined by Dynamic Mechanical Thermal Analysis, along with improved thermal stability. In contrast, the torrefied rice husk composites based on PHB showed similar tensile and flexural moduli but demonstrated lower tensile strength, reduced elongation, and decreased flexural yield stress compared to unfilled PHB.

However, only a limited number of studies have focused on composites incorporating torrefied hemp biomass[24,25], and, to the best of our knowledge, no detailed investigation has yet been conducted on the fabrication, characterization, and performance of PLA-based composites reinforced with torrefied hemp hurd. Furthermore, although existing studies tend to emphasize the mechanical and thermal properties of such composites, there is a gap in the literature concerning their tribological behavior-particularly referring to their wear resistance - that is relevant for engineering applications across diverse industrial sectors.

In this contest, hemp hurd was subjected to torrefaction at three temperatures (namely, 220 °C, 260 °C, and 300 °C) with the primary objective of enhancing its hydrophobic characteristics and improving its compatibility with a poly(lactic acid) (PLA) matrix. This thermal pre-treatment was aimed at improving the wear resistance and mechanical performance of PLA-based composites without the need for additional chemical or physical surface modifications. Composite formulations were prepared with two different weight fractions of hemp hurd, namely 2.5 wt% and 5.0 wt%. For comparison, analogous composites incorporating untreated (non-torrefied) hemp hurd were also prepared and investigated. A characterization of the thermally modified hemp hurd was conducted using scanning electron microscopy (SEM), wide-angle X-ray diffraction (WAXD), attenuated infrared spectroscopy (ATR), and proximate analysis to assess changes in morphology, crystalline structure, and compositional attributes induced by torrefaction. The interfacial adhesion between the PLA matrix and the hemp hurd filler within the composite materials was examined via SEM analysis. Ensuing analyses focused on evaluating the structural, thermal, and mechanical properties of the composites, as well as their tribological behavior. These properties were compared to those of the reference composite containing untreated hemp hurd and the unfilled polymer, to elucidate the effects of torrefaction treatment on the overall performance of the resulting composites.

Materials and methods

Materials

PLA 2003D was supplied by Ingeo™ NatureWorks (Minnesota, MN, USA). 2003D is a high molecular weight extrusion grade, typically used as part of a formulated blend. Hemp Hurd (HH) raw material used for this work was wasted hemp, recovered from the shredding process employed in the textile industry.

Methods

Torrefaction process

Batch torrefaction tests were carried out in a laboratory-scale fluidized bed reactor (40 mm inner diameter) at 220, 260, and 300 °C, setting the reaction time to 15 min. The torrefaction operating conditions were selected based on our previous fluidized bed torrefaction studies on agro-industrial residues[26–28] and on the characteristic thermal decomposition behavior of raw hemp hurd determined through thermogravimetric analysis. Briefly, a relatively short residence time of 15 min was adopted to take advantage of the enhanced heat transfer characteristics of fluidized beds, which allow a significant reduction in the reaction time (from the typical 30–120 min required in more conventional fixed or rotary drum reactors) while still achieving satisfactory torrefaction performance. The selected operative temperatures allow for comprehensive evaluation across the entire torrefaction severity spectrum, from mild (220 °C) to more severe (300 °C) conditions, ensuring optimal process insight and

appropriate selection of the torrefied solid for the subsequent application. The TG and DTG curves of hemp hard (described in more detail in 3.1.3. Thermochemical analysis of the raw and torrefied hemp hurds) exhibit distinct stages of thermal degradation that guided the temperature selection. In particular: (a) 220 °C represents the onset decomposition temperature of hemp hurd, corresponding to the initial decomposition of hemicellulose and the beginning of the torrefaction regime. At this temperature, the DTG curve shows the start of the major decomposition peak, ensuring mild torrefaction conditions while ensuring high mass yields; (b) 260 °C was selected as it corresponds to the peak temperature for hemicelluloses decomposition, appearing as a shoulder on the main DTG curve. This temperature, where hemicellulose degradation is most active while cellulose decomposition remains limited, provides an optimal balance between mass loss and energy densification; (c) 300 °C represents the end of the primary torrefaction regime, where hemicellulose decomposition is nearly complete and cellulose degradation becomes more pronounced. This temperature ensures more severe torrefaction conditions while remaining below the onset of extensive feedstock decomposition, which occurs above 320 °C.

Commercial γ-alumina powder (Souter mean diameter ≈ 150 µm) was employed as a bed material. This choice was motivated by comprehensive operational and economic considerations derived from our previous fluidized bed torrefaction studies[27](Brachi et al. 2017; 2019). γ-Alumina powder (ρ_p = 1250 kg/m³) has significantly lower density compared to conventional silica sand (ρ_p = 2650 kg/m³), resulting in smoother bed fluidization and reduced minimum fluidization velocity. This enhanced fluidization behavior enables higher biomass-to-inert ratios in the bed while maintaining stable fluidization conditions (with no segregation phenomena), thereby improving process economics through increased feedstock throughput per unit of bed material. Additionally, the superior fluidization characteristic of γ-alumina reduces carrier gas requirements compared to sand beds, contributing to lower operating costs. Furthermore, γ-alumina demonstrates excellent thermal stability and maintains its structural integrity and surface properties through the torrefaction temperature range.

Before torrefaction, the raw-HH sample was sieved, and the 1.40–2.36 mm size fraction was selected for testing. In a typical experimental run, the biomass loading in the bed was set to approximately 10 wt%. Nitrogen was introduced at about 375 Nl/h to guarantee complete fluidization of the γ-Al_2O_3/HH binary mixture and hence to obtain a uniform solid product[28]. At the end of the set 15-minute treatment time, the torrefied solid was rapidly discharged and quenched by connecting a stainless steel vacuum chamber to the fluidized bed reactor. Repeated tests were performed to produce sufficient torrefied material (30–40 g) for the subsequent characterizations and testing.

After torrefaction, the color of hemp hurd particles changed as a function of the treatment severity (i.e., mostly the temperature, see Fig. 1), in agreement with previous observations that darker color correlates with higher conversion and mass loss[26]. The torrefied samples then were ground in a batch knife mill at 5500 rpm to obtain particles smaller than 500 µm, as required for subsequent characterizations and testing. The three torrefied samples are referred to as HH220, HH260, and HH300, corresponding to their respective treatment temperatures.

Fig. 1. Appearance of hemp hurd after the torrefaction process, before and after grinding. Torrefaction process was performed at (**a**) 220 °C, (**b**) 260 °C, and (**c**) 300 °C.

Characterization of torrefied materials

Raw and torrefied biomass samples were analyzed using different techniques to assess how torrefaction conditions affect the properties of the solid product. The morphology of the raw and thermally treated materials was examined by scanning electron microscopy (SEM, Nova NanoSEM 450-FEI).

XRD measurements were performed using a Rigaku MiniFlex 600 diffractometer. The X-ray generator was equipped with a copper tube operating at 40 kV and 15 mA. XRD spectra were acquired at ambient temperature over the 2θ range of 3°–90° with a 0.01° step width and a scan speed of 10.00°/min. The crystallinity index (CI) of the cellulosic fractions was derived from the diffractograms as the height ratio between the intensity of the crystalline peak (I_{002}–I_{am}) and total intensity (I_{002}) after subtraction of the background signal measured without cellulose, in line with the following equation proposed by Segal et al.[29,30]:

$$CI_{xrd}(\%) = \frac{I_{002} - I_{am}}{I_{002}} \times 100 \quad (1)$$

where I_{002} was the intensity of the 002 crystalline peak at 22° and I_{am} the height of the minimum (I_{am}) between the 002 and the 101 peaks.

Proximate analysis was carried out using a thermogravimetric analyzer (TGA 701 LECO). The elemental composition (C, H, N) was determined using a LECO CHN 2000 analyzer, while the oxygen content was obtained by difference, by subtracting the ash and the CHN contribution from 100%. All these tests were made at least in triplicate. The higher heating value (HHV, MJ/kg, db) was estimated by the unified empirical correlation (Eq. 2) proposed by Channiwala and Parikh[31]:

$$HHV\left(\frac{MJ}{kg},\ db\right) = \frac{349.1C + 1178.3H - 103.4O - 15.1N - 21.1ASH}{1000} \quad (2)$$

where C, H, O, N and ASH are the weight fraction (wt%) of carbon, hydrogen, oxygen, nitrogen, and ash as determined by ultimate analysis on a dry basis. The lower heating values (LHV, MJ/kg, db) were obtained from the HHV by subtracting the latent heat associated with water vapor in the combustion products, according to Eq. (3):

$$LHV\left(\frac{MJ}{kg},\ db\right) = HHV\left(\frac{MJ}{kg},\ db\right) - 2.442 \times \frac{8.936\,H}{100} \quad (3)$$

where the constant 2.442 is the enthalpy difference in MJ/kg between steam and liquid water at 25 °C, the constant 8.936 is the ratio of the molar mass of water (H_2O) to that of hydrogen (H_2) and finally, H is the weight fraction (wt%) of hydrogen in the sample on a dry basis.

The thermal degradation behavior of raw and torrefied hemp hurd samples was investigated using a PerkinElmer STA 6000 simultaneous thermal analyzer. Approximately 10 g of sample was heated from room temperature up to 935 °C under nitrogen (80 ml/min) at a heating rate of 5 °C/min.

FTIR spectra of both untreated and torrefied hemp fibers were collected using a Nicolet 5700 spectrometer (Thermo Scientific, Waltham, USA) equipped with an attenuated total reflectance (ATR) accessory (SmartOrbit, Thermo Scientific). Spectra were acquired between 500 and 4000 cm^{-1} with a resolution of 2 cm^{-1}.

Preparation of the PLA-based composites

PLA-based composites were produced by melt mixing in a Brabender W50E internal mixer (Plasti-Corder, Duisburg, Germany) operated at 170 °C and 100 rpm for 5 min. The composites contained 2.5 and 5 wt% of each torrefied filler. Unfilled PLA was processed under similar conditions as a reference material. Prior to compounding, PLA pellets and filler powders were vacuum-dried overnight at 65 °C. The compounded materials were subsequently compression molded by using a Collin P200T laboratory press (Maitenbeth, Germany) at 170 °C, applying a pressure of 100 bar for 5 min. The composites were indicated in this paper using the code wHHx, where "w" represents the filler loading (in wt%) and "x" denotes the torrefaction temperature. Rectangular specimens measuring 70 × 70 × 0.5 mm^3 were prepared for tensile testing. Portions of these samples were also used for microstructural and thermal characterizations. For tribological testing, rectangular specimens with dimensions of 30 × 30 × 5 mm^3 were employed.

Characterization of the PLA-based composites

The cross-sectional morphology and dispersion of torrefied hemp hurd biochar within the PLA matrix were examined using a ZEISS EVO 50 XVP scanning electron microscope (SEM; Oberkochen, Germany). To avoid plastic deformation during fracture, the spacimens were cutted in liquid nitrogen. SEM observations were also performed after the tribological tests on worn surfaces. Prior to imaging, all specimens were sputter-coated with a 10 nm thick gold layer to reduce electrostatic charging. The effect of filler incorporation on the structure of PLA was investigated by wide-angle X-ray diffraction (WAXD) using an X'Pert PRO MPD PW3040/60 diffractometer (PANalytical, Malvern, UK), which operated in Bragg-Brentano geometry. X-ray radiation was generated by a high-power ceramic tube (PW3373/10 LFF) equipped with a copper anode (Kα radiation, λ = 0.15418 nm) working at 45 kV and 40 mA. WAXD patterns were collected in continuous scan mode at a scanning rate of 0.04°/s over a 2θ range of 5–50°.

Thermal properties of the composites were characterized by differential scanning calorimetry (DSC) and thermogravimetric analysis (TGA). DSC measurements were performed on approximately 6 mg of each

sample using a DSC Q20 calorimeter (TA Instruments, New Castle, DE, USA) to determine the glass transition temperature (T_g), crystallization temperature (T_c), and melting temperature (T_m). Measurements were performed in triplicate. The analyses were conducted with a three-step thermal program at a heating rate of 10 °C/min: (i) first heating from 0 °C to 200 °C, (ii) cooling from 200 to 0 °C, and (iii) second heating from 0 to 200 °C.

Thermal stability was assessed using a PerkinElmer STA 6000 thermal analyzer. Approximately 10 mg of each material was heated from 30 °C to 700 °C at a rate of 10 °C/min under both air and nitrogen atmospheres, with a flow rate of 80 mL/min. Tensile properties were evaluated using an Instron 5966 universal testing machine (Norwood, MA, USA). Specimens had dimensions of 40 mm in length, 5 mm in width, and 0.5 mm in thickness. Tests were carried out at room temperature at a constant crosshead speed of 2 mm/min until break. Tensile strength (σ_β), elongation at break (ε), and Young's modulus (E) were determined as average values from at least ten specimens for each sample.

Hardness measurements were performed in accordance with ASTM D2240 using a Shore D Classic Durometer (Sauter, Wutoschingen, Germany). Ten measurements were taken for each specimen to ensure reproducibility.

The tribological performance of PLA and composites was investigated by ball-on-disc wear testing by using a CSEM tribometer (Alpnach, Switzerland). An alumina (Al_2O_3) ball with a diameter of 6 mm was employed as the counterbody. Tests were conducted at room temperature under a normal load of 7 N and a sliding speed of 10 cm/s, with a rotational radius of 5 mm. The total sliding distance was 1100 m, corresponding to 35.000 cycles. The reported COF values represent mean ± standard deviation of three measurements. Volume loss and track depth were quantified using a Form Talysurf 120 contact profilometer (Taylor Hobson, Leicester, UK). Wear volume was determined by integrating the cross-sectional area of the wear track derived from three-dimensional surface profile. The Archard wear model was used for calculating the specific wear rate (K, $mm^3/m\ N$):

$$K = \frac{V}{S * L} \tag{4}$$

where V is the wear volume (mm^3), S is the final sliding distance (m) and L is the applied load during the test[32].

Results and discussion

Torrefied hemp hurd

Morphological analysis of the raw and torrefied hemp hurd

The morphological features of raw hemp hurd and its torrefied derivatives are presented in Fig. 2. The raw hemp hurd (Fig. 2A) exhibits a fibrous structure with fiber diameters ranging from 10 to 30 µm. As well known, the outer layer exhibits a rough texture consisting of cellulose, hemicellulose, and lignin, surrounding an inner core primarily composed of cellulose.

Torrefaction induces gradual structural degradation of the raw material. At a torrefaction temperature of 220 °C (Fig. 2B), the fibrous structure is partially disrupted, and a three-dimensional porous architecture is visible. As the treatment temperature increases to 260 °C (Fig. 2C), the structure begins to collapse, becoming more fragile. At 300 °C (Fig. 2D), a complete structural breakdown is observed, resulting in the formation of thin, flake-like sheets. These flakes exhibit well-defined pores, likely due to the release of volatile compounds during the high-temperature thermal decomposition process.

Structural analysis of the raw and torrefied hemp hurds

The X-ray diffractograms of the raw and thermally treated hemp hurd samples are shown in Fig. 3. Both the raw and the torrefied samples exhibit a diffraction pattern similar to that of cellulose, which is characterized by the presence of three main peaks and a broad amorphous background band. The main peak, observed at $2\theta = 22.5°$, is related to the 200 crystallographic plane, whereas the broad peak at lower angle is the result of the overlapping of the diffraction peak at $2\theta = 15.0°$ and 16.5°, both related to the 110 plane[33,34]. The third peak, observed at $2\theta = 34.5°$, is assigned to the 004 crystalline plane[35]. The main peak at $2\theta = 22.5°$ was used for the calculation of the crystallinity index (CI).

Crystallinity index (collected in Table 1) exhibits first an apparent increase moving from the raw feedstock to the one treated at the lowest temperature of 220 °C (i.e., starting from 58.6% to 61.3%) and then a decrease that becomes more pronounced at the highest treatment temperature of 300 °C (i.e., 59.7% for the HH260 and 40.3% for HH300). Taking into account that about 58.6% of the raw feedstock polysaccharides are crystalline and the remaining constituents are amorphous (i.e., hemicelluloses, pectic substances, amorphous regions of the cellulose fibrils), it is likely to assume that the observed initial increase of CI can be attributed to the biomass degradation caused by torrefaction, which, at first, reduces the amorphous fraction of hemp hurd; consequently, an increase in the relative crystalline content is observed. The subsequent thermal degradation steps, involving both the amorphous and the crystalline fraction, lead to a gradual and then sharp collapse of the overall crystallinity of the material. This result confirms what was observed by morphological analysis, where it is evident that the increase in processing temperature leads to the destruction of the three-dimensional aspect of hemp hurd, originally consisting of lignocellulosic structures that are still clearly visible for HH220.

Thermochemical analysis of the raw and torrefied hemp hurds

The TG and dTG thermograms of the raw and the thermally treated hemp hurd samples, obtained under a nitrogen atmosphere at a heating rate of 5 °C/min are collected in Fig. 4. The data highlight that the raw hemp hurd sample (HH0) exhibits the typical thermogravimetric behavior of a standard lignocellulosic biomass (mainly composed of hemicellulose, cellulose, and lignin), namely characterized by the presence of three main decomposition stages. The first one (represented by the first peak on the dTG curve), which occurs at temperatures below 150 °C, is ascribed to the removal of water and some low molecular weight organic volatiles[35].

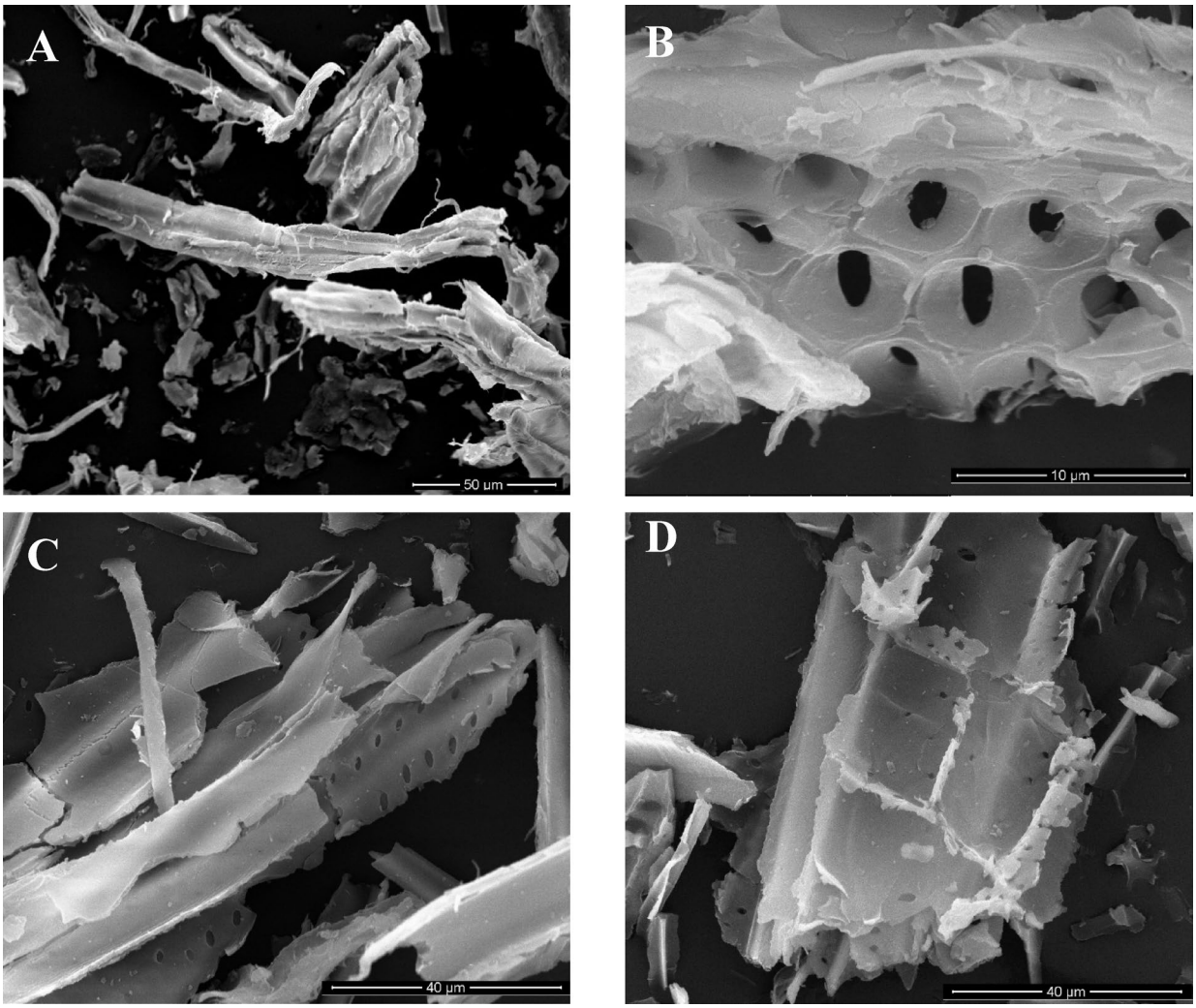

Fig. 2. Scanning Electron Microscopy (SEM) micrographs of (**A**) raw hemp hurds, and the same material following torrefaction at (**B**) 220 °C, (**C**) 260 °C, and (**D**) 300 °C. The analysis was conducted on ground materials.

The second decomposition stage, which extends over the temperature range from 150 to approximately 350 °C and accounts for about 65 wt% of the total mass loss could mainly be ascribed to the thermal decomposition of holocellulose (hemicellulose and cellulose) macromolecules. The latter, in particular, typically occurs through the two sequential and partially overlapping degradation steps of hemicelluloses (the shoulder peak), which typically decompose in the range of 220–280 °C, and of cellulose (the main peak), which typically occurs in the range of ca. 275–400 °C[36]. Finally, the third decomposition stage covering the temperature range from 350 to approximately 935 °C corresponds to the slow (namely without a characteristic peak) weight loss of the lignin whose decomposition typically occurs over a broad temperature range (ca. 160–900 °C)[36] in light of the different thermal stability of the several oxygen functional groups present in its structure[37]. A decomposition profile similar to that of the untreated sample (HH0) was also observed in the case of the torrefied solids, except for the reduced amplitude of the peaks relative to the first pyrolysis stage, particularly at the highest torrefaction operating temperature. This finding is consistent with experimental evidence that mass loss during torrefaction mainly comes from the hemicellulose decomposition and partly from the beginning of cellulose decomposition[38].

The chemical composition and the heating values of the raw and thermally treated samples are reported in Table 1. As expected, the volatile matter (VM) and the oxygen content in the thermally-treated samples decrease with the increase of treatment severity (i.e., increasing the processing temperatures), whereas the carbon, the fixed carbon (FC), and the ash contents increase. The HH composition changes led by torrefaction also results in a rise of the calorific value of torrefied solids with respect to the parent one. Specifically, it results that the higher the torrefaction temperature, the higher the calorific values (HHV and LHV) of the solid product. Figure 5 shows the results of the ultimate and proximate analyses in terms of the O/C and H/C atomic ratios (mol/mol) on a dry, ash-free basis (daf) in the Van Krevelen diagram. This diagram shows that as the temperature level adopted during thermal treatment increases, the composition of the samples shifts from the region characteristic of biomass to that of low-rank fossil solid fuels, such as peat and lignite.

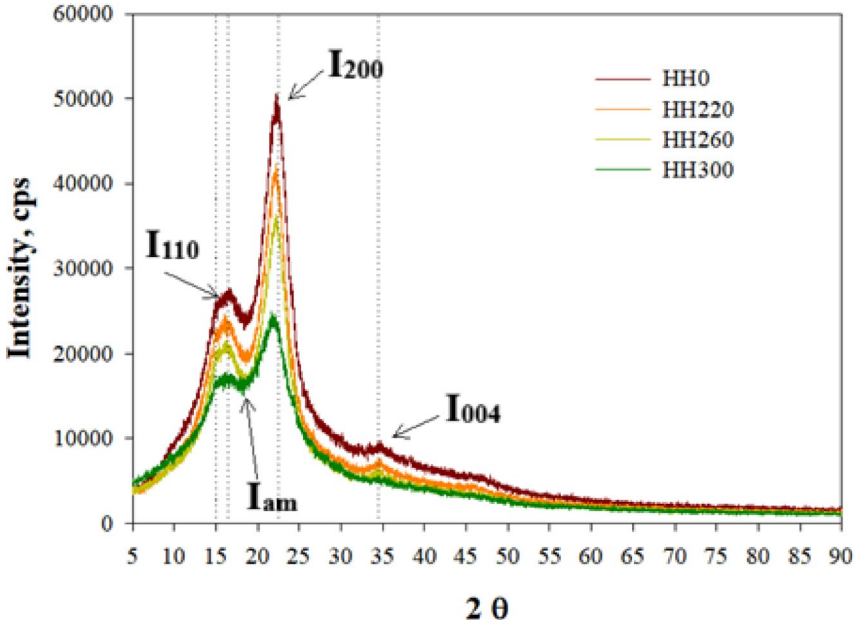

Fig. 3. X-ray diffractograms of raw and torrefied hemp hurd samples.

	HH0	HH220	HH260	HH300
Cristallinity index	58.6	61.3	59.7	40.3
Moisture (wt%, as received)				
Proximate analysis (wt%, dry basis)	9.78	3.92	4.05	4.21
Volatile matter	80.82	78.76	72.37	57.62
Fixed carbon	16.87	18.98	24.76	37.82
Ash	2.31	2.25	2.86	4.56
Ultimate analysis (wt%, dry basis)				
C	45.09	47.21	51.22	56.61
H	5.63	6.04	5.81	5.06
N	0.93	0.29	0.28	0.36
O (by diff.)	46.03	44.21	39.84	33.41
HHV (MJ/kg, dry basis)	17.56	18.97	20.54	22.17
LHV (MJ/kg, dry basis)	16.33	17.65	19.27	21.06

Table 1. Cristallinity index, proximate, ultimate and calorific analyses of raw and torrefied hemp hurd (HH).

Figure 6 presents the averaged ATR spectra (ranging from 4000 to 500 cm^{-1}) of untreated and treated hemp hurd at each torrefaction temperature (220, 260, or 300 °C).

The broad band at 3600–3200 cm^{-1}, present in all the spectra, can be associated with the stretching of O–H groups mostly involved in intra- and inter-molecular hydrogen bonds. It is reported that this band becomes weaker with increasing torrefaction temperatures because of the degradation of hemicellulose and cellulose and it disappears when the degradation has been completed[39]. The analysis of FTIR fingerprint region (1800–650 cm^{-1}) gives relatively similar spectra. However, it can be observed that the C=O stretching band at 1730 cm^{-1} becomes broad and shifts to lower wavenumbers increasing the torrefaction temperature (1693 cm^{-1} at 290 °C). This indicates that the starting of hemicellulose and cellulose degradation occurs between 250 and 280 °C[40]. The intensity of lignin band at 1263 cm^{-1} (aromatic C–O stretching of methoxyl units), decreases at high temperatures as lignin degrades[40,41], while the intensity of the peak at 1506 cm^{-1} (aromatic C=C ring vibration) remains unchanged. Additional spectral changes in lignin-associated bands include a progressive increase in the intensity of the C=C stretching vibration peak at 1599 cm^{-1}. The prominent C–O band at 1022 cm^{-1} is assigned to cellulose and hemicelluloses and decreases in intensity with increasing torrefaction temperature[41]. This means that the degradation of main components in the hemp biomass increases with the torrefaction temperature but is not completed, and the filler continues to be hydrophilic in a way that is a function of the torrefaction process.

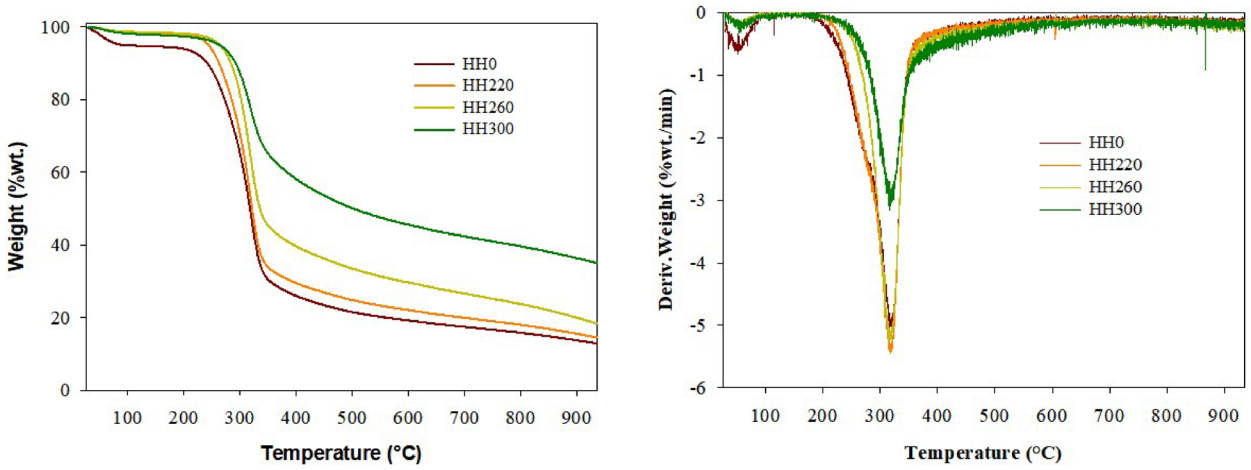

Fig. 4. TG and dTG curves of raw (HH0) and torrefied hemp hurds, recorded at 5 °C/min under nitrogen atmosphere with a purge rate of 80 ml/min from RT to about 935 °C.

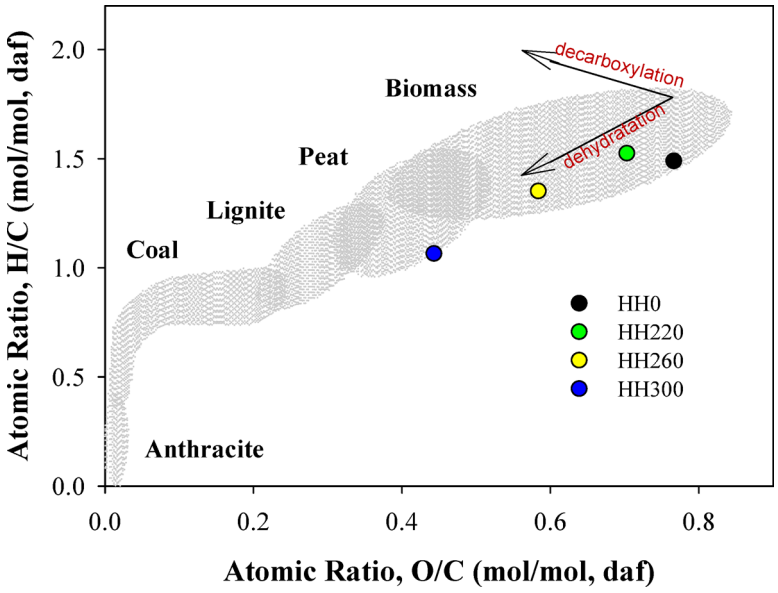

Fig. 5. Van Krevelen diagram of raw and torrefied hemp hurd samples.

Characterization of PLA-based composites

Morphological analysis of the PLA-based composites

Figure 7 presents SEM micrographs of the cross-sections of PLA-based composites incorporating untreated and torrefied hemp hurd. For HH0 (Fig. 7A and B), a non-uniform dispersion of the filler within the PLA matrix is observed. Large particles exceeding 200 µm surrounded by big voids (indicated by red arrows) suggests poor adhesion between the two phases. HH220 composites show the original three-dimensional structure with characteristic lignocellulosic channels discernible in both longitudinal and transverse sections, indicating limited structural disruption. Moreover, poor interfacial adhesion between the polymer and the filler is evident, particularly in Fig. 7C (sample 5.0HH220), where numerous voids (red arrows) are observed. These voids are attributed to the detachment of thermally treated particles during the fracture of the composite material. Improved dispersion is observed for the HH260 composites (Fig. 7E and F). In this case, the presence of smaller, well-distributed filler particles (highlighted by the blue arrows) suggests a reduction in aggregation. As previously shown in Fig. 2C, the partial degradation of the lignocellulosic structure during torrefaction at 260 °C likely facilitated more effective dispersion during the melt mixing process. Nevertheless, the interfacial bonding between the PLA matrix and HH260 remains weak, as indicated by the presence of voids (red arrows) resulting from particle detachment upon fracture.

The highest dispersion quality is achieved with HH300 at both compositions, as illustrated in Fig. 7G and H. The number of detachment voids (red arrows) is reduced, suggesting improved polymer/filler affinity, as

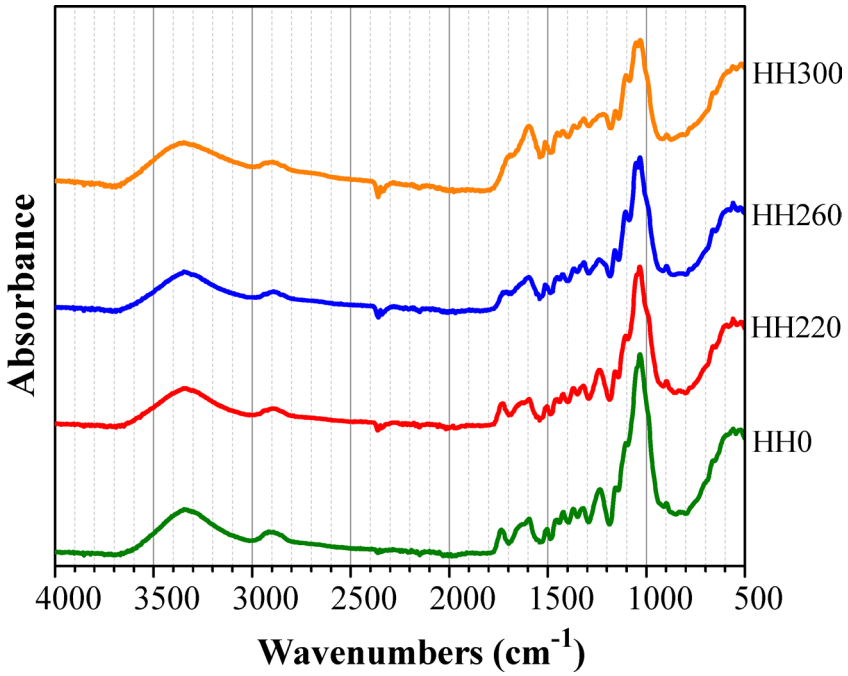

Fig. 6. ATR-FTIR spectra (4000–650 cm^{-1}) for control (hemp hurd not torrefied) and chips torrefied at 220, 260, and 300 °C.

also demonstrated by ultimate analysis (i.e., the oxygen content in the torrefied solids decreases with increasing temperature, whereas the carbon increases-see Table 1).

Structural analysis of the PLA-based composites

PLA can crystallize into for different forms (namely, α, α', β, or γ forms[42,43], according to the preparation method. Because of its inherently slow crystallization kinetics, it typically remains amorphous under conventional melt processing characterized by high cooling rates[44]. PLA displays an amorphous structure as indicated by a broad scattering pattern in Fig. 8. It is characterized by the superposition of two halos centered at 2θ values of 16.5° and 20.4°. This scattering behavior is similar to that observed for PET by Murthy et al.[45] and has also been observed in PLA. It suggests the existence of two distinct interchain spacings, as described by Stoclet et al.[46]. The presence of both untreated and torrefied hemp hurd does not induce any crystallization phenomena. The diffractograms of all the composites show two main peaks as unfilled PLA, the first of which, however, is shifted to lower 2θ values and presents a higher relative intensity with respect to the second one, indicating that the fillers are interacting with the polymer matrix in a way that alters its local packing structure.

Thermal properties of the PLA-based composites

The DSC thermograms of unfilled PLA and its composites are presented in Fig. 9 and the thermal parameters are collected in Table 2. During the first heating, PLA (black curves) showed a T_g of 61.7 °C, followed by an endothermic peak attributable at the cold crystallization phenomenon (T_{cc} = 111.9 °C). The melting behavior shows two peaks at 151 °C and 155 °C. The lower temperature peak typically corresponds to the melting of the less-ordered crystalline regions, while the higher temperature peak represents the melting of the more organized, thicker crystals forming during the initial crystallization or through the reorganization/recrystallization process during heating[47,48]. During the cooling run, it was possible to observe only the T_g step that occurred at 55.5 °C. The absence of an endothermic peak related to the PLA crystallization phenomenon indicates that the polymer cannot crystallize at the cooling rate used for the DSC experiment. During the second heating, PLA shows a T_g slightly lower with respect to the first heating (60.9 °C instead of 61.7 °C), whereas the T_{cc} of the second heating run is slightly higher than the first heating (113.4 °C instead of 111.9 °C). No substantial differences between first and second run are observed in the temperature and shape of the peak related to the T_m.

For each composite, it is observed that the T_g of the first heating is higher than the T_g of the second heating, as that the T_{cc} of the second heating is higher than the T_{cc} of the first heating. The T_g values of the composites are generally comparable to that of unfilled PLA, with the exception of the HH0 samples, which exhibit a reduction of approximately 3 °C during the first heating cycle. Also, for the composites, the cooling condition does not allow the crystallization of PLA (i.e., only the T_g is observed during the cooling down). Although slight variations in the thermal parameters are observed, these variations do not seem to be influenced by the temperature employed for obtaining HH. Only in the case of the T_{cc} the composites show a lower T_{cc} than that observed for the unfilled PLA, both in the first and in the second heating up. This result may indicate that the presence of HH promotes the cold crystallization process at a lower temperature, acting as a nucleating agent of PLA[49,50]; further, this effect

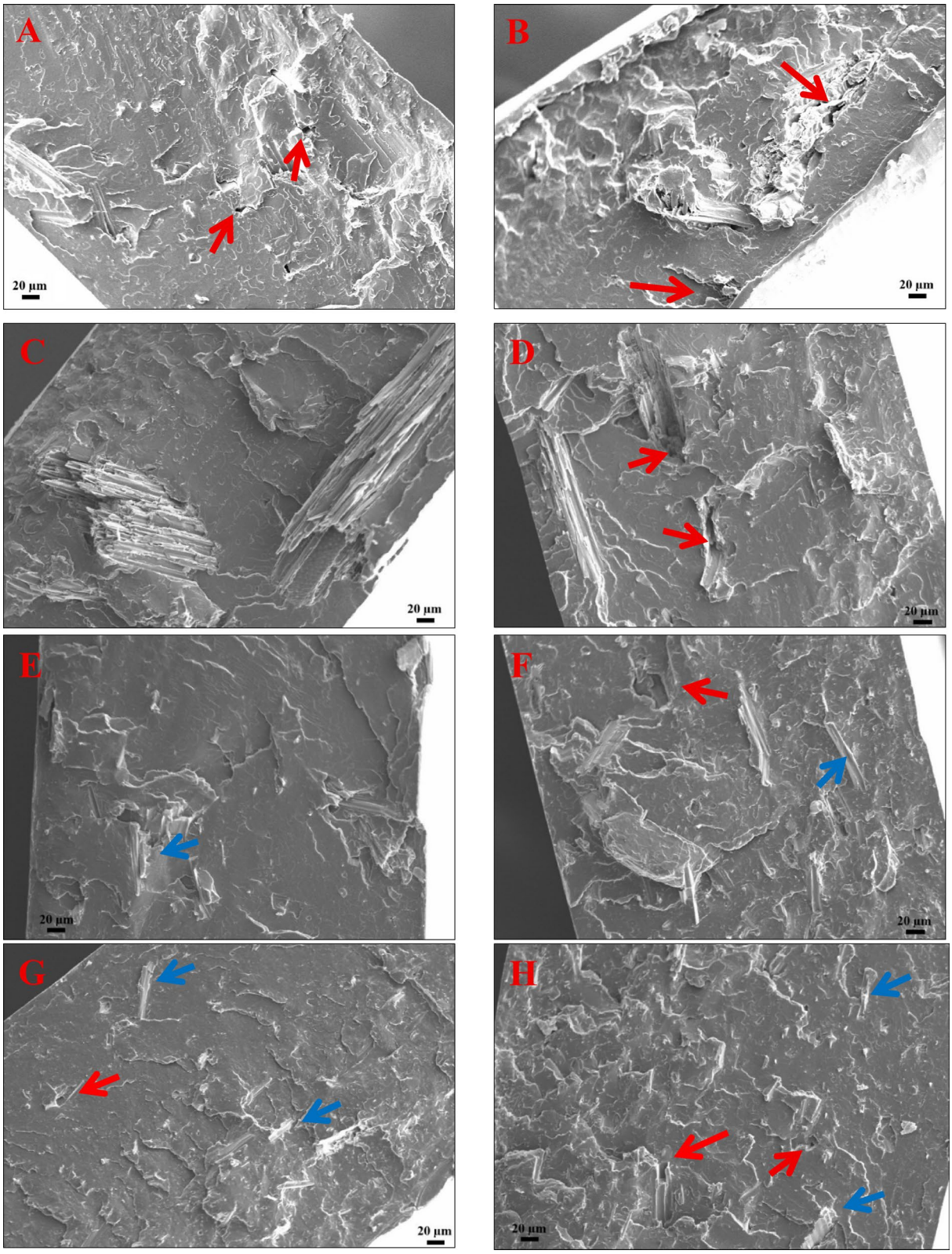

Fig. 7. SEM micrographs of the cross section of (**A**) 2.5HH0, (**B**) 5.0HH0, (**C**) 2.5HH220, (**D**) 5.0HH220, (**E**) 2.5HH260, (**F**) 5.0HH260, (**G**) 2.5HH300, (**H**) 5.0HH300.

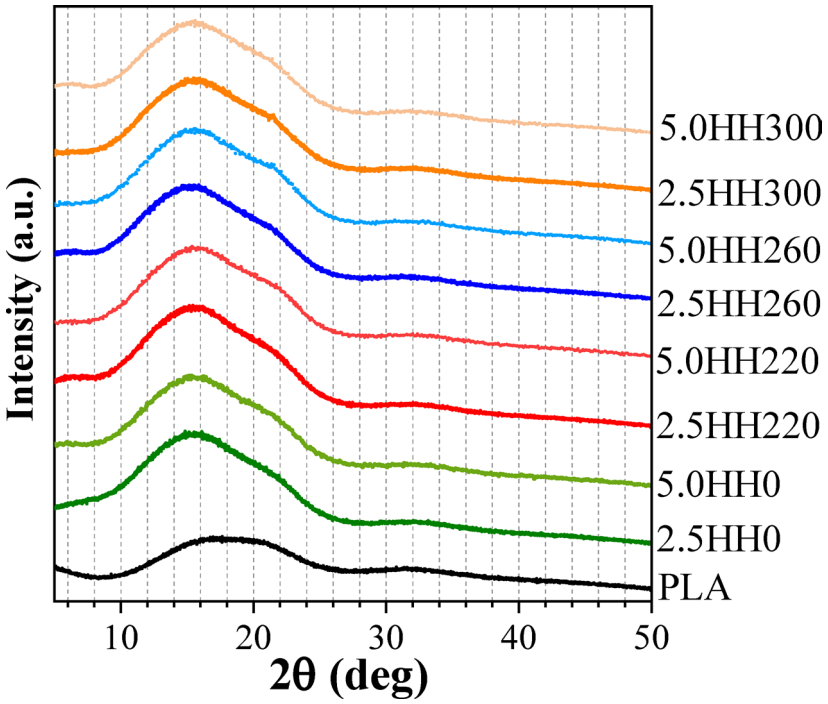

Fig. 8. WAXD patterns of neat PLA and the PLA/hemp hurd composites.

is more pronounced by increasing the HH torrefaction temperature. This is also consistent with the findings of Berthet et al.[18] for PHBV reinforced with torrefied lignocellulosic fibers.

The thermogravimetric (TG) and its derivative (dTG) curves of PLA and its composites under a nitrogen atmosphere are presented in Fig. 10, with the corresponding thermal degradation parameters summarized in Table 3. Unfilled PLA exhibited initial (T_{10}) and half-weight loss (T_{50}) temperatures of 357 °C and 368 °C, respectively. The dTG curve revealed a single degradation peak with a maximum decomposition temperature (T_{max}) of 360 °C, which corresponds to the degradation of the polymer matrix[51]. As shown in Fig. 10 and detailed in Table 3, all PLA composites display a shift of the main degradation peak toward lower temperatures. This shift became more pronounced with increasing HH content, indicating a decrease in the thermal stability of the composites. This behavior can be attributed to the lower thermal degradation temperature of lignocellulosic fillers and is consistent with trends commonly reported for PLA-based composites reinforced with lignocellulosic fillers[52–54]. Nevertheless, the thermal stability of the composites remains suitable for numerous applications[55].

Interestingly, the HH0 composites exhibit the lowest thermal stability among the investigated composites. A gradual improvement is observed with the use of torrefied HH, with thermal stability following the trend: HH0 < HH220 < HH260 < HH300. This enhancement is likely due to the improved compatibility between the torrefied HH and the PLA matrix at higher torrefaction temperatures, as suggested by SEM micrographs, contributing to improve the thermal performance of PLA/HH300 with respect to PLA/HH0[56,57].

Mechanical properties of the PLA-based composites

The stress-strain curve of unfilled PLA (black curve in Fig. 11) indicates that the polymer has a brittle behavior with low elongation at break (5.9%). The presence of hemp hurd (HH) inhibits the yielding behavior of PLA and significantly reduces its ductility for all the composites. When untreated hurd is incorporated (i.e., PLA/2.5HH0 and PLA/5.0HH0), all mechanical properties decline sharply, indicating poor adhesion between the hemp hurd and PLA, as confirmed by SEM analysis (Fig. 11; Table 4). In composites containing torrefied hemp hurds, an increase in Young's modulus (*E*) is observed across all formulations with respect to that of unfilled PLA, as often reported in literature[17,19]. More specifically, the modulus increases progressively with higher hemp hurd content and high torrefaction temperatures. The sample showing the highest Young's modulus is 5.0HH300, confirming the improved polymer/filler interaction and a more homogeneous composite microstructure. This interpretation is confirmed by the results of elongation at break (ε_b) and tensile strength (σ_b). As already mentioned, the addition of HH reduces the ductility of the polymer matrix; unfilled PLA exhibits an ε_b of 5.9%, whereas the composites show values ranging from 1.4% to 2.5%. Among these, composites containing HH300 exhibit the highest ε_b values, with both 2.5HH300 and 5.0HH300 reaching 2.5%. In contrast, composites with HH0 display reduced ductility, with ε_b values of 1.7% and 1.4% for 2.5HH0 and 5.0HH0, respectively. Intermediate values are observed for HH220 and HH260 composites. A similar behavior is observed in tensile strength (σ_b). Notably, HH300 composites exhibit the highest σ_b values of about 48 MPa compared to 38 MPa for unfilled PLA. All these results suggest that HH300 enhances both strength and toughness with respect to HH0, HH220, and HH260, likely due to improved interfacial adhesion between the torrefied hemp hurd and the PLA matrix. Similar trends have been reported in the literature[23,25]. In particular, PHA composites reinforced with torrefied hemp fibers[25]

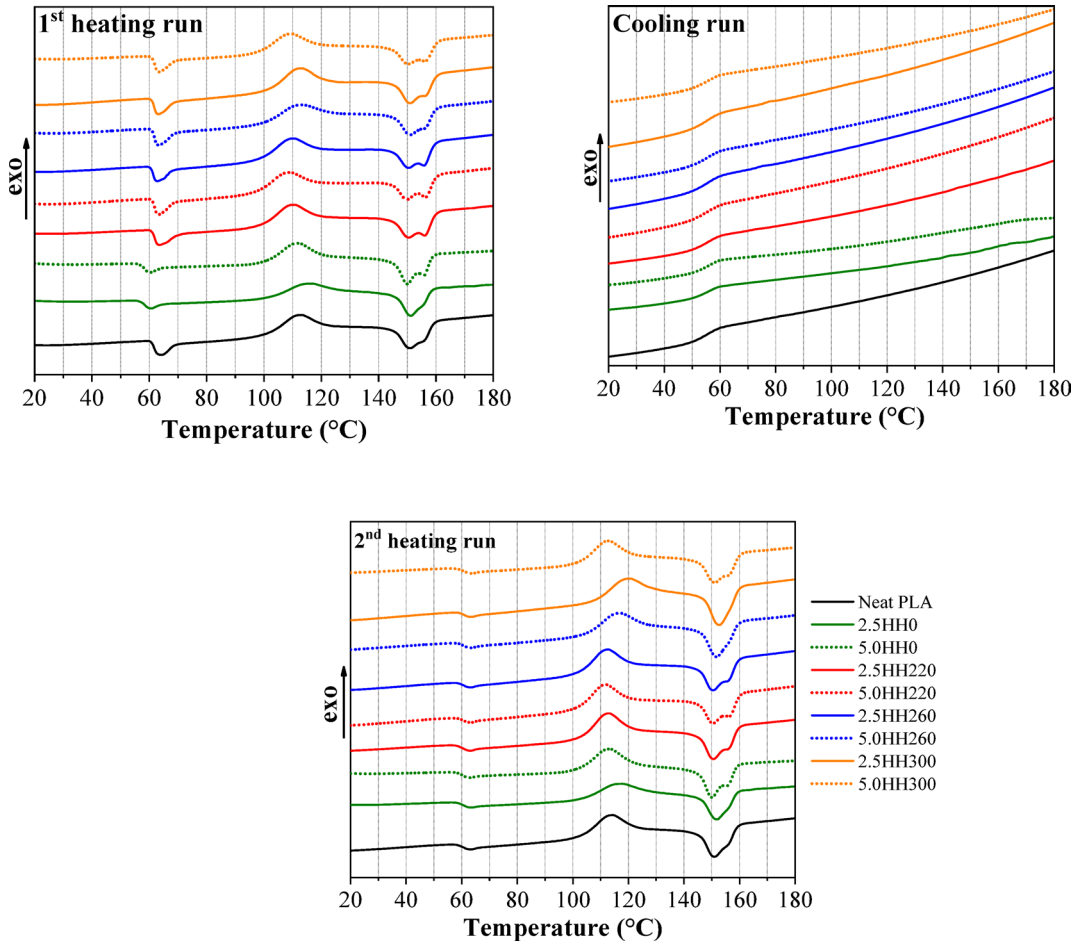

Fig. 9. DSC curves of unfilled PLA and its composites (1st heating run: 0 to 200 °C, at 10 °C/min; Cooling run: from 200 to 0 °C, at 10 °C/min; 2nd heating run: from 0 to 200 °C, at 10 °C/min).

	1st heating			2nd heating			Cooling
	T_g (°C)	T_{cc} (°C)	T_m (°C)	T_g (°C)	T_{cc} (°C)	T_m (°C)	T_g (°C)
Unfilled PLA	61.7 ± 0.8	111.9 ± 1.0	155.5 ± 0.8	60.9 ± 0.5	113.4 ± 1.2	156.0 ± 1.2	55.5 ± 0.8
2.5 HH0	58.7 ± 0.8	114.8 ± 0.9	155.70 ± 0.3	60.6 ± 0.1	115.8 ± 1.3	155.9 ± 1.9	55.7 ± 0.7
5.0HH0	58.5 ± 0.5	111.3 ± 1.1	155.7 ± 0.3	60.8 ± 0.3	112.7 ± 1.4	155.6 ± 1.5	56.6 ± 0.7
2.5HH220	61.9 ± 0.4	109.5 ± 0.9	156.4 ± 0.4	60.6 ± 0.4	112.5 ± 1.4	156.2 ± 1.2	55.3 ± 0.9
5.0HH220	61.9 ± 0.9	108.0 ± 1.2	156.6 ± 0.7	60.6 ± 0.3	111.4 ± 1.6	156.3 ± 1.2	56.1 ± 0.2
2.5HH260	61.4 ± 0.7	109.3 ± 1.1	156.1 ± 0.6	60.9 ± 0.2	112.2 ± 1.8	155.8 ± 1.3	55.7 ± 0.6
5.0HH260	61.8 ± 0.6	111.7 ± 1.4	156.5 ± 0.7	61.2 ± 0.4	115.7 ± 1.4	151.8 ± 1.7	55.6 ± 0.3
2.5HH300	61.7 ± 0.2	113.2 ± 0.9	156.4 ± 0.3	61.2 ± 0.2	120.5 ± 1.4	152.8 ± 1.8	55.2 ± 0.9
5.0HH300	61.9 ± 0.6	102.7 ± 0.6	156.4 ± 0.3	60.7 ± 0.3	112.3 ± 1.9	156.5 ± 1.8	55.0 ± 1.0

Table 2. Thermal parameters from DSC for neat PLA and its composites.

showed substantial improvements in mechanical properties compared to the neat polymer, including increases of 211% in tensile modulus, 55% in tensile strength, 361% in flexural modulus, and 329% in flexural strength, as the torrefaction temperature increased[23]. A comparable behavior was observed in PLA composites reinforced with torrefied yellow poplar, where higher torrefaction temperatures also led to enhanced strength.

The hardness (Shore D) of unfilled PLA and its composites is also collected in Table 4. As already observed for the tensile strength, the addition of HH increased the hardness of the composites. HH300 increased this property to a greater extent than the other HH. In detail, unfilled PLA shows a hardness of 90.9, while 5.0HH300 presents the highest hardness value, namely 96.0.

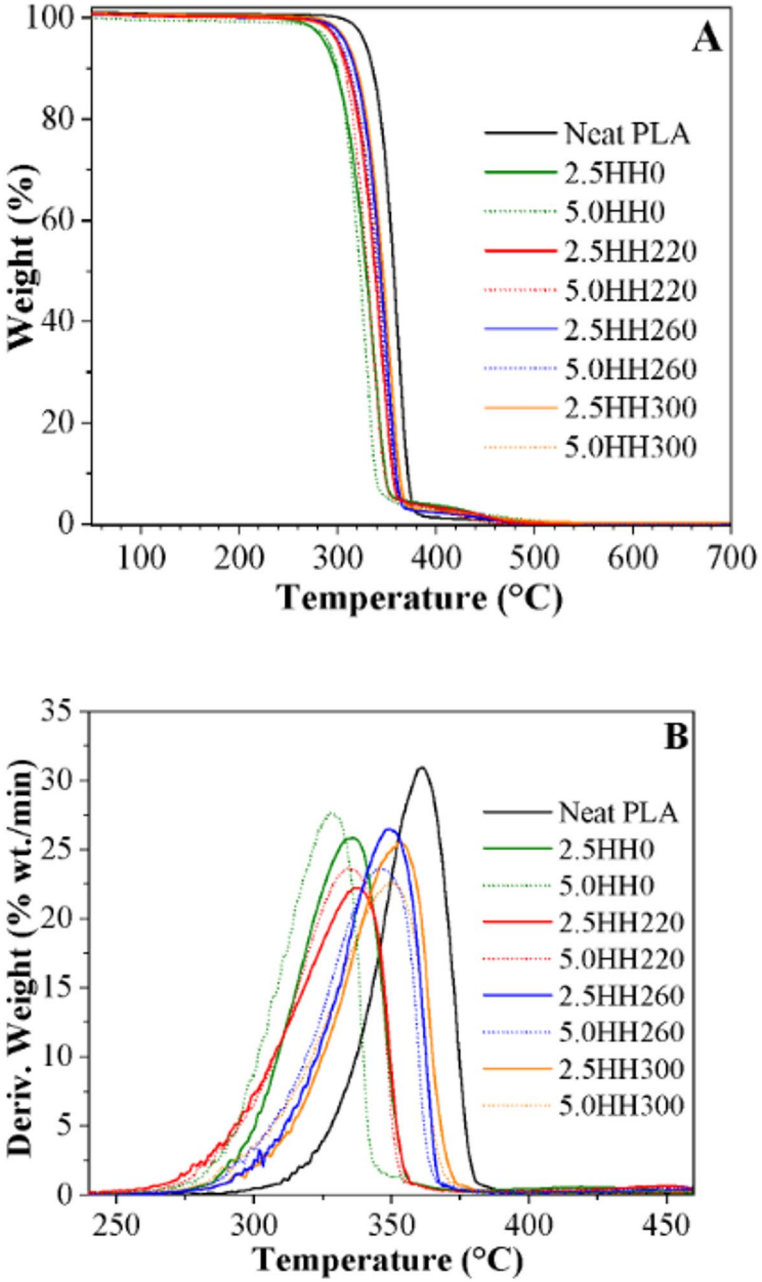

Fig. 10. TG (**A**) and dTG (**B**) curves of neat PLA and its composites performed under nitrogen atmosphere (heating rate: 10 °C/min).

Tribological behavior of the PLA-based composites

Unfilled PLA, HH0 composite, and all composites containing 2.5 wt% of torrefied hemp hurd exhibit a similar COF profile (Fig. S1 in the supplementary section). These samples display a running-in phase lasting approximately 150–200 m, after which a steady-state friction regime is established. In this regime, COF values range from 0.491 for unfilled PLA to 0.391 for the 2.5HH260 composite (Table 4). Additionally, stick-slip behavior, which is commonly observed in the tribological testing of polymers[58], is evident in all of these samples. These findings indicate that the incorporation of untreated hemp hurd or low (2.5 wt%) loadings of torrefied hurd does not significantly alter the frictional response of the PLA matrix. A substantial change in COF behavior is, however, observed when the torrefied filler content increases to 5.0 wt% (Fig. 12; Table 4). Indeed, in these composites, the COF reaches steady-state values without a distinct running-in period. Moreover, the steady-state COF is significantly reduced, ranging from 0.110 for 5.0HH260 to 0.083 for 5.0HH300: this finding highlights the strong influence of filler loading and torrefaction temperature on the COF values. These results could be ascribed to the increase in the carbonaceous content in the filler (as demonstrated by ultimate analysis), possessing self-lubricating properties, stabilizing the coefficient of friction, and also reducing wear loss[59]. In fact, unfilled PLA shows a W_s of 7.2 10^{-4} mm^3/N m, which increases to 8.3 10^{-4} mm^3/N m for 2.5HH0-based composites and to

	$T_{10\%}$ (°C)	$T_{50\%}$ (°C)	T_{max} (°C)	Residue @ 700 °C (%)
Unfilled PLA	335 ± 3	357 ± 2	360 ± 2	0
2.5HH0	307 ± 2	330 ± 2	335 ± 4	0
5.0HH0	299 ± 3	323 ± 3	328 ± 3	0
2.5HH220	298 ± 4	329 ± 1	337 ± 2	0.2
5.0HH220	301 ± 2	326 ± 2	335 ± 1	0
2.5HH260	317 ± 3	343 ± 1	349 ± 1	0
5.0HH260	312 ± 1	340 ± 2	346 ± 2	0
2.5HH300	319 ± 2	346 ± 1	353 ± 4	0.3
5.0HH300	310 ± 4	342 ± 1	350 ± 1	0.2

Table 3. Thermogravimetric data for unfilled PLA and its composites.

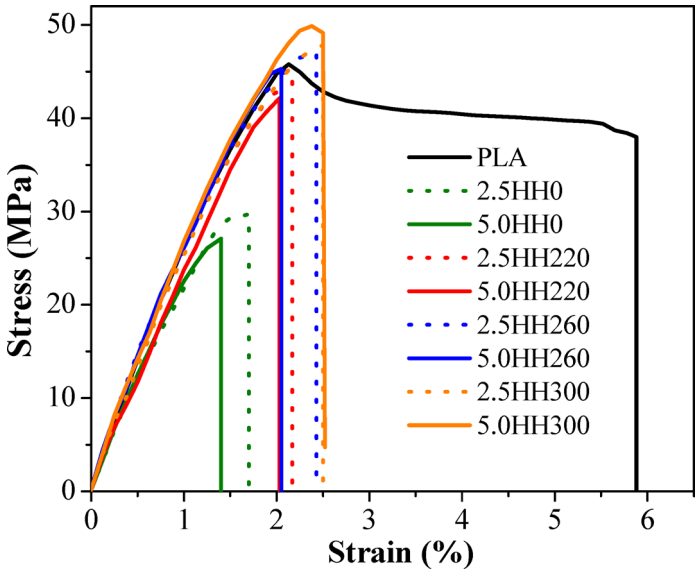

Fig. 11. Stress–strain curves of unfilled PLA and its composites.

	E (MPa)	ε_b (%)	σ_b (MPa)	H (Shore D)	COF	WR ($mm^3/N{\cdot}m){\cdot}10^{-4}$	d_{max} (µm)
Unfilled PLA	2972 ± 115	5.9 ± 3.1	38.0 ± 4.8	90.9 ± 3.1	0.491 ± 0.013	7.2	141 ± 18
2.5HH0	2691 ± 69	1.7 ± 0.4	29.7 ± 6.3	90.5 ± 3.0	0.418 ± 0.014	8.5	166 ± 22
5.0HH0	2673 ± 79	1.4 ± 0.4	27.1 ± 5.9	92.7 ± 2.3	0.405 ± 0.011	7.3	139 ± 16
2.5HH220	3064 ± 62	2.2 ± 0.2	43.9 ± 2.2	91.9 ± 2.3	0.445 ± 0.012	7.7	143 ± 19
5.0HH220	3139 ± 145	2.0 ± 0.2	42.2 ± 4.1	94.3 ± 3.7	0.107 ± 0.008	0.013	0.83 ± 0.09
2.5HH260	3105 ± 118	2.4 ± 0.2	46.9 ± 2.6	93.8 ± 2.9	0.391 ± 0.009	5.7	121 ± 11
5.0HH260	3220 ± 68	2.1 ± 0.2	45.3 ± 2.2	94.5 ± 3.1	0.110 ± 0.010	0.011	0.95 ± 0.09
2.5HH300	3215 ± 75	2.5 ± 0.2	47.8 ± 2.1	93.3 ± 3.3	0.464 ± 0.012	5.3	113 ± 12
5.0HH300	3341 ± 142	2.5 ± 0.1	48.4 ± 3.0	96.0 ± 2.5	0.083 ± 0.002	0.008	0.87 ± 0.08

Table 4. Mechanical and tribological parameters of unfilled PLA and its composites. Young modulus (E), tensile strength (σb), elongation at break (εb), hardness (H), friction coefficient (COF), specific wear rate (WR) and the maximum depth (dmax) were reported in the table.

7.7 mm^3/N m when 2.5 wt% of HH220 is incorporated into PLA. The W_s value slightly decreases for 2.5HH260 and 2.5HH300 (i.e., 5.7 and 5.3, respectively). The W_s observed for the composites prepared with 5.0 wt% of torrefied hemp hurd is significantly lower than those observed for the previously discussed samples and for 5.0HH0. Specifically, the wear rate is 0.013, 0.011, and 0.008 mm^3/N m for samples 5.0HH220, 5.0HH260, and 5.0HH300, respectively. Similarly, the maximum depth (d_{max}) for unfilled PLA, HH0 composites, and the composites containing 2.5 wt% of torrefied hemp hurd ranges from 113 to 166 µm, while samples containing 5.0

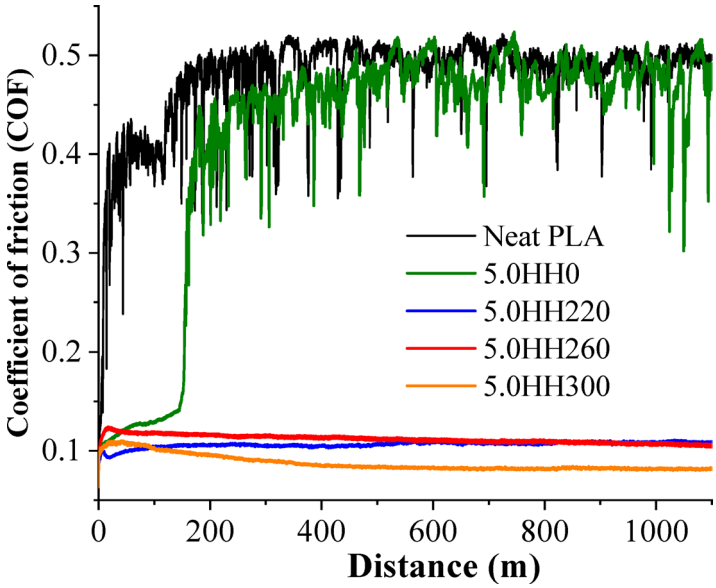

Fig. 12. Evolution of the friction coefficient (COF) during the tribological test, performed on unfilled PLA and its composites containing 5 wt% of HH torrefied at different temperatures.

wt% of the torrefied filler exhibit significantly lower values, ranging from 0.83 to 0.95 μm. This highlights the protective effect exerted by the torrefied material against wear loss.

The wear track of the unfilled PLA, observed by SEM (Fig. 13A), is approximately 1.8 mm wide, and the surface of the track does not appear excessively damaged by debris. The smoothness of this surface suggests that the main wear mechanism of the material under test conditions could involve the formation of a polymeric transfer layer from the polymer to the alumina ball counterpart. This layer is promoted by adhesion phenomena occurring at the interface that, during sliding, induces shear stresses in the contact zone[60]. As it can be seen in Fig. 13B, C and D, and 13E, this phenomenon remains unchanged for the materials filled with 2.5 wt% of untreated and torrefied hemp hurd; however, the wear tracks appear less wide, particularly for 2.5HH260 and 2.5HH300. In these images, the formation of surface cracks due to the presence of the filler is also evidenced by red circles. Figure 13F shows the wear track for 5.0HH300 sample. The surface of the track is smooth and significantly shallower and narrower with respect to the other composites, confirming the ability of the torrefied hemp hurd to limit the transfer process from the sample to the alumina ball. This reduction in friction and wear can also be ascribed to the improved load-bearing capacity (increased hardness and stiffness of the composites)[58,59]. As an example, Fig. 13G shows the micrograph of the alumina ball used for the tribological test on 2.5HH300 (all the other alumina ball surfaces are reported in Fig. S2 in the supplementary section). Although the surface is not worn due to the soft counterface, it shows the presence of adhering PLA material.

Conclusions

In this study, hemp hurd was torrefied at three temperatures: 220 °C, 260 °C, and 300 °C. This thermal pretreatment was intended to enhance the properties of PLA composites, such as wear resistance and mechanical properties, without requiring additional surface modifications. Composites were produced with a hemp hurd content of 2.5 and 5 wt%, alongside reference samples containing untreated filler, for comparison. The torrefaction of hemp hurd provided an effective and sustainable strategy to enhance the performance of PLA-based composites. Composites containing 5 wt% of HH300 exhibited the most notable improvements, including high stiffness, tensile strength, hardness, and wear resistance with respect to both unfilled PLA and untreated hemp hurd-based composites. SEM analysis revealed that higher torrefaction temperatures resulted in better dispersion and interfacial adhesion, which accounted for enhanced mechanical properties and reduced wear. The tribological benefits were attributed to the formation of a polymeric transfer layer and to improved load-bearing capacity (increased hardness and stiffness of the composites). Overall, incorporating torrefied hemp hurd, especially when processed at 300 °C, represents a viable route toward creating more durable and sustainable PLA-based materials.

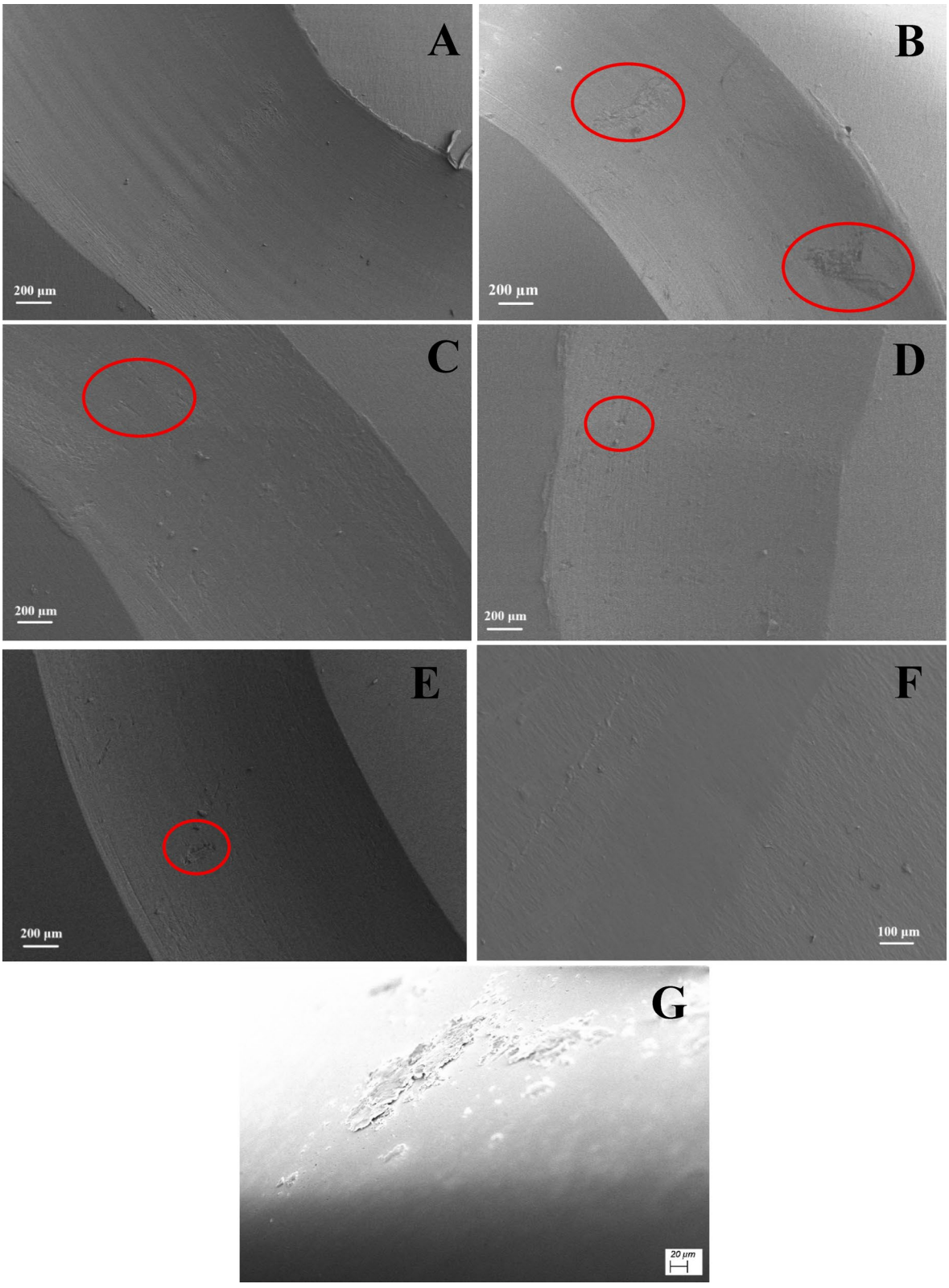

Fig. 13. SEM micrographs of worn surfaces of (**A**) neat PLA, (**B**) 2.5HH0 (**C**) 2.5HH220, (**D**) 2.5HH260, (**E**) 2.5HH300 and (**F**) 5.0HH300. (**G**) Alumina ball used for the tribological measurements on 2.5HH300.

Data availability

The data that support the findings of this study are available from the corresponding author upon reasonable request.

Received: 16 March 2026; Accepted: 26 April 2026
Published online: 09 May 2026

References

1. Ely, K., Podder, S., Reiss, M. & Fike, J. Industrial Hemp as a crop for a sustainable agriculture. in *Cannabis/Hemp for Sustainable Agriculture and Materials* (eds Agrawal, D. C., Kumar, R. & Dhanasekaran, M.) (Springer, Singapore, 2022). https://doi.org/10.1007/978-981-16-8778-5_1.
2. Visković, J. et al. Industrial hemp (*Cannabis sativa* L.) agronomy and utilization. *Rev. Agron.* **13**, 931. https://doi.org/10.3390/agronomy13030931 (2023).
3. Crini, G., Lichtfouse, E., Chanet, G. & Morin-Crini, N. Traditional and new applications of hemp. *Sustain. Agri Rev.* **42**, 37–87. https://doi.org/10.1007/978-3-030-41384-2_2 (2020).
4. Basak, M. et al. A critical review of industrial fiber hemp anatomy, agronomic practices, and valorization into sustainable bioproducts. *BioResources* **20**(2), 5030–5070. https://doi.org/10.15376/biores.20.2.Basak (2025).
5. Duraccio, D. et al. Improving wear resistance of epoxy resin using bio-oil from hemp biomass: A sound strategy to reduce environmental impact. *J. Clean. Prod.* **495**, 145003. https://doi.org/10.1016/j.jclepro.2025.145003 (2025).
6. Agyemang, E., Ofori-Dua, K., Dwumah, P. & Forkuor, J. B. Towards responsible resource utilization: A review of sustainable vs. unsustainable reuse of wood waste. *PLoS ONE*. **19**, e0312527. https://doi.org/10.1371/journal.pone.0312527 (2024).
7. Teuber, L., Osburg, V. S., Toporowski, W., Militz, H. & Krause, A. Wood polymer composites and their contribution to cascading utilization. *J. Clean. Prod.* **110**, 9–15. https://doi.org/10.1016/j.jclepro.2015.04.009 (2016).
8. Mohanty, A., Misra, M. A. & Hinrichsen, G. Biofibres, biodegradable polymers and biocomposites: An overview. *Macromol. Mater. Eng.* **276**, 1–24. https://doi.org/10.1002/(SICI)1439-2054(20000301)276:1<1::AID-MAME1>3.0.CO;2-W (2000).
9. Khan, B. A. Development of Antibacterial Hemp Hurd/Poly(Lactic Acid) Biocomposite for Food Packaging. PhD Thesis (University of Southern Queensland, Australia, 2017).
10. Li, X., Xiao, R., Morrell, J. J., Zhou, X. & Du, G. Improving the performance of hemp hurd/polypropylene composites using pectinase pre-treatments. *Ind. Crops Prod.* **97**, 465–468. https://doi.org/10.1016/j.indcrop.2016.12.061 (2017).
11. Essabir, H. et al. Bio-composites based on polypropylene reinforced with almond shells particles: Mechanical and thermal properties. *Mater. Des.* **51**, 225–230. https://doi.org/10.1016/j.matdes.2013.04.031 (2013).
12. Bokhari, S. M., Chi, K. & Catchmark, J. M. Structural and physico-chemical characterization of industrial hemp hurd: Impacts of chemical pretreatments and mechanical refining. *Ind. Crops Prod.* **171**, 113818. https://doi.org/10.1016/j.indcrop.2021.113818 (2021).
13. Stevulova, N. et al. Properties characterization of chemically modified hemp hurds. *Materials* **7**, 8131–8150. https://doi.org/10.3390/ma7128131 (2014).
14. Chiou, B. S. et al. Torrefaction of almond shells: Effects of torrefaction conditions on properties of solid and condensate products. *Ind. Crops Prod.* **86**, 40–48. https://doi.org/10.1016/j.indcrop.2016.03.030 (2016).
15. Soponpongpipat, N., Sittikul, D. & Sae-Ueng, U. Higher heating value prediction of torrefaction char produced from non-woody biomass. *Front. Energy.* **9**, 461–471. https://doi.org/10.1007/s11708-015-0377-3 (2015).
16. Sarker, T. R., Nanda, S., Dalai, A. K. & Meda, V. A review of torrefaction technology for upgrading lignocellulosic biomass to solid biofuels. *BioEnergy Res.* **14**, 645–669. https://doi.org/10.1007/s12155-020-10236-2 (2021).
17. Vold, J. J. L., Ulven, C. A. & Chisholm, B. J. Torrefied biomass filled polyamide biocomposites: Mechanical and physical property analysis. *J. Mater. Sci.* **50**, 725–732. https://doi.org/10.1007/s10853-014-8632-2 (2014).
18. Berthet, M. A., Commandré, J. M., Rouau, X., Gontard, N. & Angellier-Coussy, H. Torrefaction treatment of lignocellulosic fibres for improving fibre/matrix adhesion in a biocomposite. *Mater. Des.* **92**, 223–232. https://doi.org/10.1016/j.matdes.2015.12.034 (2016).
19. McCaffrey, Z. et al. Recycled polypropylene-polyethylene torrefied almond shell biocomposites. *Ind. Crops Prod.* **125**, 425–432. https://doi.org/10.1016/j.indcrop.2018.09.012 (2018).
20. Chiou, B. S. et al. Torrefied biomass-polypropylene composites. *J. Appl. Polym. Sci.* **132**, 41582. https://doi.org/10.1002/app.41582 (2015).
21. Ortiz-Barajas, D. L., Arévalo-Prada, J. A., Fenollar, O., Rueda-Ordóñez, Y. J. & Torres-Giner, S. Torrefaction of coffee husk flour for the development of injection-molded green composite pieces of polylactide with high sustainability. *Appl. Sci.* **10**, 6468. https://doi.org/10.3390/app10186468 (2020).
22. McCaffrey, Z. et al. Polyhydroxybutyrate Rice Hull and Torrefied Rice Hull biocomposites. *Polymers* **14**, 3882. https://doi.org/10.3390/polym14183882 (2022).
23. Giang, D. K. et al. Effect of torrefied biomass on hydrophobicity and mechanical properties of polylactic acid composite. *Int. J. Biol. Macromol.* **215**, 36–44. https://doi.org/10.1016/j.ijbiomac.2022.06.084 (2022).
24. Vold, J. L. L. *Microwave torrefaction of natural fibers for incorporation into engineering thermoplastic biocomposites* (Diss. North Dakota State University, 2015).
25. Lim, H. et al. Torrefied hemp fiber as a sustainable reinforcement for biodegradable PHA composites: Enhancing interfacial compatibility and environmental stability. *Comp. Part. B Eng.* **304**, 112653. https://doi.org/10.1016/j.compositesb.2025.112653 (2025).
26. Brachi, P., Chirone, R., Miccio, M. & Ruoppolo, G. Fluidized bed torrefaction of commercial wood pellets: Process performance and solid product quality. *Energy Fuels.* **32**, 9459–9469. https://doi.org/10.1021/acs.energyfuels.8b01519 (2018).
27. Brachi, P., Chirone, R., Miccio, F., Miccio, M. & Ruoppolo, G. Valorization of orange peel residues via fluidized bed torrefaction: comparison between different bed materials. *Combust. Sci. Technol.* **191**, 1585–1599. https://doi.org/10.1080/00102202.2019.1582526 (2019).
28. Del Duca, V. et al. Binary mixtures of biomass and inert components in fluidized beds: experimental and neural network exploration. *Fuel* **346**, 128314. https://doi.org/10.1016/j.fuel.2023.128314 (2023).
29. Segal, L., Creely, J. J., Martin, A. E. & Conrad, C. M. An empirical method for estimating the degree of crystallinity of native cellulose using the x-ray diffractometer. *Text. Res. J.* **29**, 786–794. https://doi.org/10.1177/004051755902901003 (1959).
30. Park, S., Baker, J. O., Himmel, M. E., Parilla, P. A. & Johnson, D. K. Cellulose crystallinity index: measurement techniques and their impact on interpreting cellulase performance. *Biotechnol. Biofuels*. https://doi.org/10.1186/1754-6834-3-10 (2010).
31. Channiwala, S. A. & Parikh, P. P. A. Unified correlation for estimating HHV of solid, liquid and gaseous fuels. *Fuel* **81**, 1051–1063. https://doi.org/10.1016/s0016-2361(01)00131-4 (2002).
32. Bhushan, B. *Introduction to Tribology* 2nd edn, pp. 56–82 (A John Wiley and Sons, Ltd., 2013).
33. Daicho, K., Saito, T., Fujisawa, S. & Isogai, A. The crystallinity of nanocellulose: Dispersion-induced disordering of the grain boundary in biologically structured cellulose. *ACS Appl. Nano Mater.* **1**, 5774–5785. https://doi.org/10.1021/acsanm.8b01438 (2018).
34. Grząbka-Zasadzińska, A., Ratajczak, I., Król, K., Woźniak, M. & Borysiak, S. The influence of crystalline structure of cellulose in chitosan-based biocomposites on removal of Ca(II), Mg(II), Fe(III) ion in aqueous solutions. *Cellulose* **28**, 5745. https://doi.org/10.1007/s10570-021-03899-3 (2021).
35. Chen, W. H. & Kuo, P. C. A study on torrefaction of various biomass materials and its impact on lignocellulosic structure simulated by a thermogravimetry. *Energy* **35**, 2580–2586. https://doi.org/10.1016/j.energy.2010.02.054 (2010).

36. D'Acierno, F., Michal, C. A. & MacLachlan, M. J. Thermal stability of cellulose nanomaterials. *Chem. Rev.* **123**, 7295–7325. https://doi.org/10.1021/acs.chemrev.2c00816 (2023).
37. Li, C., Zhao, X., Wang, A., Huber, G. W. & Zhang, T. Catalytic transformation of lignin for the production of chemicals and fuels. *Chem. Rev.* **115**, 11559–11624. https://doi.org/10.1021/acs.chemrev.5b00155 (2015).
38. Meng, J., Park, J., Tilotta, D. & Park, S. The effect of torrefaction on the chemistry of fast-pyrolysis bio oil. *Bioresour. Technol.* **111**, 439. https://doi.org/10.1016/j.biortech.2012.01.159 (2012).
39. Rudolfsson, M., Borén, E., Pommer, L., Nordin, A. & Lestander, T. A. Combined effects of torrefaction and pelletization parameters on the quality of pellets produced from torrefied biomass. *Appl. Energy*. **191**, 414. https://doi.org/10.1016/j.apenergy.2017.01.035 (2017).
40. So, C. L. & Eberhardt, T. L. FTIR-based models for assessment of mass yield and biofuel properties of torrefied wood. *Wood Sci. Technol.* **52**, 209. https://doi.org/10.1007/s00226-017-0970-1 (2017).
41. Zheng, A. et al. Impact of torrefaction on the chemical structure and catalytic fast pyrolysis behavior of hemicellulose, lignin, and cellulose. *Energy Fuels*. **29**, 8027. https://doi.org/10.1021/acs.energyfuels.5b01765 (2015).
42. Sasaki, S. & Asakura, T. Helix distortion and crystal structure of the α-form of poly(L-lactide). *Macromolecules* **36**, 8385–8390. https://doi.org/10.1021/ma0348674 (2003).
43. Zhang, J., Tashiro, K., Tsuji, H. & Domb, A. J. Disorder-to-order phase transition and multiple melting behavior of poly(l-lactide) investigated by simultaneous measurements of WAXD and DSC. *Macromolecules* **41**, 1352–1357. https://doi.org/10.1021/ma0706071 (2008).
44. Tabi, T., Sajo, I. E., Szabo, F., Luyt, A. S. & Kovacs, J. G. Crystalline structure of annealed polylactic acid and its relation to processing. *Express Polym. Lett.* **4**, 659–668. https://doi.org/10.3144/expresspolymlett.2010.80 (2010).
45. Murthy, N. S., Correale, S. T. & Minor, H. Structure of the amorphous phase in crystallizable polymers: Poly(ethylene terephthalate). *Macromolecules* **24**, 1185–1189 (1991).
46. Stoclet, G., Seguela, R., Lefebvre, J. M., Elkoun, S. & Vanmansart, C. Strain-induced molecular ordering in polylactide upon uniaxial stretching. *Macromolecules* **43**, 1488–1498. https://doi.org/10.1021/ma9024366 (2010).
47. Wei, L. L. et al. Effect of a phosphorus-containing flame retardant on the thermal properties and ease of ignition of poly (lactic acid). *Polym. Degrad. Stab.* **96**, 1557. https://doi.org/10.1016/j.polymdegradstab.2011.05.018 (2011).
48. Choi, I. S. et al. Effects of polybutylene succinate content on the rheological properties of polylactic acid/polybutylene succinate blends and the characteristics of their fibers. *Materials* **17**, 662. https://doi.org/10.3390/ma17030662 (2024).
49. Yang, Z., Li, X., Si, J., Cui, Z. & Peng, K. Morphological, mechanical and thermal properties of poly (lactic acid)(PLA)/cellulose nanofibrils (CNF) composites nanofiber for tissue engineering. *J. Wuhan Univ. Technol. Mater. Sci. Ed.* **34**, 207–215. https://doi.org/10.1007/s11595-019-2037-7 (2019).
50. George, J., Jung, D. & Bhattacharyya, D. Improvement of electrical and mechanical properties of PLA/PBAT composites using coconut shell biochar for antistatic applications. *Appl. Sci.* **13**, 902. https://doi.org/10.3390/app13020902 (2023).
51. Das, O., Sarmah, A. K. & Bhattacharyya, D. Biocomposites from waste derived biochars: Mechanical, thermal, chemical, and morphological properties. *Waste Manag.* **49**, 560–570. https://doi.org/10.1016/j.wasman.2015.12.007 (2016).
52. Dong, Y. et al. Polylactic acid (PLA) biocomposites reinforced with coir fibres: Evaluation of mechanical performance and multifunctional properties. *Compos. Part. Appl. Sci. Manuf.* **63**, 76–84. https://doi.org/10.1016/j.compositesa.2014.04.003 (2014).
53. Gomez-Caturla, J. et al. Biopolypropylene-based wood plastic composites reinforced with mango peel flour and compatibilized with an environmentally friendly copolymer from itaconic acid. *ACS Appl. Polym. Mater.* **4**, 4398–4410. https://doi.org/10.1021/acsapm.2c00373 (2022).
54. De Rosa, I. M. et al. Poly(lactic acid)/phormium tenax composites: Morphology and thermo-mechanical behavior. *Polym. Compos.* **32**, 1362–1368. https://doi.org/10.1002/pc.21159 (2011).
55. Kumar, N. & Das, D. Fibrous biocomposites from nettle (*Girardinia diversifolia*) and poly(lactic acid) fibers for automotive dashboard panel application. *Compos. Part. B Eng.* **130**, 54–63. https://doi.org/10.1016/j.compositesb.2017.07.059 (2017).
56. Chen, K. et al. Effect of silane coupling agent on compatibility interface and properties of wheat straw/polylactic acid composites. *Int. J. Biol. Macromol.* **182**, 2108–2116. https://doi.org/10.1016/j.ijbiomac.2021.05.207 (2021).
57. Li, C., Liao, H., Gao, H. & Cheng, F. Enhancing interface compatibility in high-filled coal gangue/polyethylene composites through silane coupling agent mediated interface modification. *Compos. Sci. Technol.* **251**, 110546. https://doi.org/10.1016/j.compscitech.2024.110546 (2024).
58. Bartoli, M. et al. Mechanical, electrical, thermal and tribological behavior of epoxy resin composites reinforced with waste hemp-derived carbon fibers. *J. Mater. Sci.* **57**, 14861–14876. https://doi.org/10.1007/s10853-022-07550-9 (2022).
59. Faga, M. G. et al. Ethylene-vinyl acetate (EVA) containing waste hemp-derived biochar fibers: Mechanical, electrical, thermal and tribological behavior. *Polymers* **14**, 4171. https://doi.org/10.3390/polym1419417 (2022).
60. Onodera, T. et al. Structure and function of transfer film formed from PTFE/PEEK polymer blend. *J. Phys. Chem. C.* **121**, 14589–14596. https://doi.org/10.1021/acs.jpcc.7b02860 (2017).

Author contributions

Conceptualization: Paola Brachi, Mattia Di Maro, Donatella Duraccio; Methodology: Paola Brachi, Mattia Di Maro, Donatella Duraccio; Formal analysis and investigation: Paola Brachi, Mattia Di Maro; Writing - original draft preparation: Paola Brachi, Mattia Di Maro; Writing—review and editing: all authors; Funding acquisition: Paola Brachi, Giovanna Ruoppolo, Donatella Duraccio; Resources: Paola Brachi, Giovanna Ruoppolo, Maria Giulia Faga, Giulio Malucelli, Donatella Duraccio; Supervision: Paola Brachi, Giovanna Ruoppolo, Maria Giulia Faga, Giulio Malucelli, Donatella Duraccio.

Funding

This work is funded by the European Union, under the project BioPhenom (101135107). Views and opinions expressed are however those of the author(s) only and do not necessarily reflect those of the European Union or the European Research Executive Agency (REA). Neither the European Union nor the granting authority can be held responsible for them.

Declarations

Competing interests

The authors declare no competing interests.

Additional information

Supplementary Information The online version contains supplementary material available at https://doi.org/1

0.1038/s41598-026-51164-z.

Correspondence and requests for materials should be addressed to M.M.